

# Majorana-Kondo interplay in T-shaped double quantum dots

I. Weymann,<sup>1,\*</sup> K. P. Wójcik,<sup>2,3,†</sup> and P. Majek<sup>1</sup>

<sup>1</sup>*Faculty of Physics, Adam Mickiewicz University,  
ul. Uniwersytetu Poznaskiego 2, 61-614 Poznań, Poland*

<sup>2</sup>*Institute of Molecular Physics, Polish Academy of Sciences, ul. Smoluchowskiego 17, 60-179 Poznań, Poland*

<sup>3</sup>*Physikalisches Institut, Universität Bonn, Nussallee 12, D-53115 Bonn, Germany*

(Dated: March 15, 2022)

The transport behavior of a double quantum dot side-attached to a topological superconducting wire hosting Majorana zero-energy modes is studied theoretically in the strong correlation regime. It is shown that the Majorana zero energy mode can leak through the dot directly attached to topological superconductor to the side attached dot, giving rise to a subtle interplay between the two-stage Kondo screening and the half-fermionic nature of Majorana quasiparticles. In particular, the coupling to the topological wire is found to reduce the effective exchange interaction between the two quantum dots in the absence of normal leads. Interestingly, it also results in an enhancement of the second-stage Kondo temperature when the normal leads are attached. Moreover, it is shown that the second stage of the Kondo effect can become significantly modified in one of the spin channels due to the interference with the Majorana zero-energy mode, yielding the low-temperature conductance equal to  $G = G_0/4$ , where  $G_0 = 2e^2/h$ , instead of  $G = 0$  in the absence of the topological superconducting wire. Finally, in the case of a short wire, a finite overlap between the wave functions of the Majorana quasiparticles localized at the ends of the wire suppresses the quantum interference and a regular two-stage Kondo effect is restored.

## I. INTRODUCTION

Topological states of matter are in the center of current research in condensed matter physics [1–3]. This is due to the fact that such states are robust against decoherence and are thus very promising for applications in quantum information and computation [4]. In this regard, zero-energy modes that form at the ends of one-dimensional topological superconductor provide an exciting example of topologically-protected states [5]. These states are solid-state realizations of the Majorana fermions, i.e. particles that are their own antiparticles [6, 7]. The signatures of such Majorana quasiparticles have been recently reported in a number of experiments [8–16].

It has been demonstrated that the detection of Majorana zero-energy modes can be performed by measuring the current flowing through an adjacent quantum dot [12]. It turns out that the presence of Majorana modes results in unique transport properties, including fractional values of the conductance [17–29]. Majorana quasiparticles leaking into the neighboring dot weakly coupled to external contacts give rise to the conductance  $G$  of the order of  $(1/4)G_0$ , where  $G_0 = 2e^2/h$  [30, 31]. On the other hand, in the strong coupling regime, the Majorana-Kondo interplay determines the transport behavior of the system [32–34]. At low temperatures, the quantum interference with a side-attached topological superconductor results in  $G = (3/4)G_0$  [33]. Such fractional values of conductance reveal a half-fermionic nature of Majorana

quasiparticles and may serve as signatures of the presence of these topologically-protected states in the system [15, 35].

In this paper we advance further the investigations of interplay between the Majorana zero-energy modes and correlations giving rise to the Kondo physics [36–38], focusing on the system built of a double quantum dot side-coupled to a Majorana wire, as schematically shown in Fig. 1. The double dot is assumed to form with external contacts a T-shaped geometry, where only one of the dots is directly coupled to the leads, while the second dot is attached indirectly through the first quantum dot. This system, in the absence of Majorana wire, is known to exhibit a nonmonotonic dependence of conductance with lowering temperature due to the two-stage Kondo effect

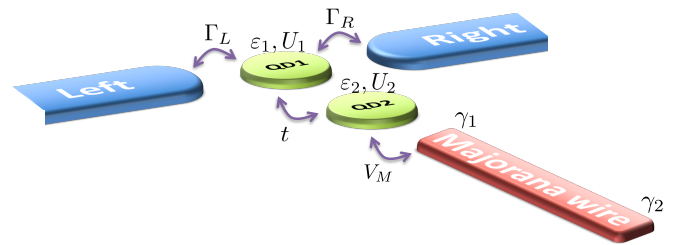


FIG. 1. The illustration of the considered system. The first quantum dot is coupled to the left and right metallic leads with coupling strengths  $\Gamma_L$  and  $\Gamma_R$ , for the left and right lead, respectively. The second quantum dot is coupled to the Majorana wire, i.e. a topological superconducting wire hosting Majorana quasiparticles described by operators  $\gamma_1$  and  $\gamma_2$ , with hopping matrix elements  $V_M$ . The two quantum dots are coupled through the hopping matrix elements  $t$ . Both dots are characterized by a single orbital level of energy  $\epsilon_j$  and Coulomb correlations  $U_j$ .

\* weymann@amu.edu.pl

† kpowojcik@ifmpan.poznan.pl

[39–44]. Moreover, the interplay between the Fano and Kondo effects in such system was shown to give rise to interesting spin-resolved transport behavior [45–47].

The main goal of this work is to uncover unique transport features resulting from the presence of Majorana quasiparticles and, in particular, to understand their influence on the two-stage Kondo effect. To achieve this goal in the most accurate way, we make use of the numerical renormalization group (NRG) method [48, 49]. We study the behavior of the spectral functions and the temperature dependence of the linear conductance, which reveal local extrema due to the leakage of Majorana quasiparticles into the double dot system. In particular, we demonstrate that the quantum interference with Majorana zero-energy mode half-suppresses the spectral features related to the second-stage Kondo effect, giving rise to the fractional value of the linear conductance  $G = (1/4)G_0$  and a unique five-peak structure in conventional transport, when the device is in the two-stage Kondo regime; cf. Ref. [28] for similar results obtained in the local singlet regime.

Furthermore, we show that, contrary to the expectations based on the analysis of excitation spectrum of double dot decoupled from normal contacts, increasing the coupling to topological superconductor actually enhances the second-stage Kondo temperature. A similar effect has been recently predicted for single quantum dots attached to Majorana wires, where an enhancement of the conventional Kondo temperature  $T_K$  was observed [26, 31, 33, 50]. In the T-shaped double quantum dot setup, at  $T < T_K$ , the spin of the second dot becomes screened by Fermi liquid formed by many-body Kondo state generated at the first quantum dot. Increasing the coupling to Majorana wire results then in an enhancement of the second-stage Kondo temperature  $T^*$ , similarly as in the single quantum dot case [26, 31, 33, 50]. Understanding this Majorana-Kondo interplay constitutes one of the main objectives of this paper.

## II. THEORETICAL DESCRIPTION

The considered system consists of a double quantum dot (DD) in a T-shaped geometry, i.e. with only one quantum dot attached directly to the leads and the second dot coupled to the first one through the corresponding hopping matrix elements. Additionally, the second quantum dot is coupled to a topological superconducting wire hosting Majorana zero-energy modes at its ends (Majorana wire). The schematic illustration of this system is presented in Fig. 1. The studied system can be described by the following Hamiltonian

$$H = H_C + H_T + H_{\text{DDM}}. \quad (1)$$

Here, the first term models the left ( $r = L$ ) and right ( $r = R$ ) metallic contacts as reservoirs of noninteracting

quasiparticles

$$H_C = \sum_{r=L,R} \sum_{\mathbf{k}\sigma} \varepsilon_{r\mathbf{k}} c_{r\mathbf{k}\sigma}^\dagger c_{r\mathbf{k}\sigma}, \quad (2)$$

where  $c_{r\mathbf{k}\sigma}^\dagger$  is the creation operator for an electron with spin  $\sigma$ , momentum  $\mathbf{k}$  and energy  $\varepsilon_{r\mathbf{k}}$  in the left ( $r = L$ ) or right ( $r = R$ ) lead. The second term of  $H$  accounts for tunneling processes between the double quantum dot-Majorana wire subsystem and the external leads. Because in the considered setup only the first dot is directly coupled to electrodes, the tunneling Hamiltonian simply reads

$$H_T = \sum_{r=L,R} \sum_{\mathbf{k}\sigma} v_r \left( d_{1\sigma}^\dagger c_{r\mathbf{k}\sigma} + c_{r\mathbf{k}\sigma}^\dagger d_{1\sigma} \right), \quad (3)$$

with the corresponding tunnel matrix elements described by  $v_r$  and assumed to be momentum independent. The operator  $d_{1\sigma}^\dagger$  ( $d_{1\sigma}$ ) is the creation (annihilation) operator of an electron with spin  $\sigma$  in the first quantum dot. The coupling to external leads gives rise to the broadening of the first dot level, which can be described by  $\Gamma_r = \pi \rho_r v_r^2$ , where  $\rho_r$  is the density of states of a given lead. In these considerations we assume a flat band of width  $2D$  for each electrode and take  $\Gamma_L = \Gamma_R \equiv \Gamma/2$ . The band halfwidth is hereafter used as the energy unit  $D \equiv 1$ .

Finally, the last term of the Hamiltonian  $H$  models the double dot-Majorana wire subsystem, and it can be written as

$$\begin{aligned} H_{\text{DDM}} = & \sum_{j=1,2} \sum_{\sigma} \varepsilon_j d_{j\sigma}^\dagger d_{j\sigma} + \sum_{j=1,2} U_j d_{j\uparrow}^\dagger d_{j\uparrow} d_{j\downarrow}^\dagger d_{j\downarrow} \\ & + \sum_{\sigma} t (d_{1\sigma}^\dagger d_{2\sigma} + d_{2\sigma}^\dagger d_{1\sigma}) \\ & + \sqrt{2} V_M (d_{2\downarrow}^\dagger \gamma_1 + \gamma_1 d_{2\downarrow}) + i \varepsilon_M \gamma_1 \gamma_2. \end{aligned} \quad (4)$$

Here,  $d_{j\sigma}^\dagger$  is the creation operator for a spin- $\sigma$  electron on dot  $j$  with the energy  $\varepsilon_j$ , and the two electrons residing on the same dot interact with the Coulomb correlation energy  $U_j$ . For the sake of clarity and convenience, we assume  $U_1 = U_2 \equiv U$ . The two quantum dots are coupled through the hopping matrix elements  $t$ . The coupling to the Majorana wire is described by the penultimate term of  $H_{\text{DDM}}$ , where  $V_M$  is the corresponding tunneling matrix element [17, 22, 33, 51]. The Majorana quasiparticles localized at the ends of the topological superconductor wire are described by the operators  $\gamma_1$  and  $\gamma_2$ . The overlap between the wave functions of these two quasiparticles is described by  $\varepsilon_M$ . When the length of the Majorana wire is much larger than the superconducting coherence length, the two Majorana quasiparticles do not overlap and, consequently,  $\varepsilon_M = 0$  [11]. In the opposite case,  $\varepsilon_M$  is finite, which results in a splitting of the energies of the Majorana quasiparticles. In the following we will refer to these two situations as the case of long/short Majorana wire.

The Majorana operators  $\gamma_1$  and  $\gamma_2$  can be represented by a fermionic operator  $f$  as  $\gamma_1 = (f^\dagger + f)/\sqrt{2}$

and  $\gamma_2 = i(f^\dagger - f)/\sqrt{2}$ , respectively. Then, the last two terms of  $H_{\text{DDM}}$  can be expressed as

$$\sqrt{2}V_M(d_{2\downarrow}^\dagger\gamma_1 + \gamma_1d_{2\downarrow}) = V_M(d_{2\downarrow}^\dagger - d_{2\downarrow})(f^\dagger + f), \quad (5)$$

$$i\varepsilon_M\gamma_1\gamma_2 = \varepsilon_M(f^\dagger f - 1/2). \quad (6)$$

In this paper we are mainly interested in the linear response transport properties of the considered Majorana-double dot structure. The linear conductance between the left and right contacts can be then found from [52]

$$G = \frac{2e^2}{h} \sum_{\sigma} \int d\omega [-f'(\omega)] \pi \Gamma A_{\sigma}(\omega), \quad (7)$$

where  $f'(\omega)$  is the derivative of the Fermi-Dirac distribution function.  $A_{\sigma}(\omega)$  denotes the spectral function of the first quantum dot for spin  $\sigma$ ,  $A_{\sigma}(\omega) = -\frac{1}{\pi} \text{Im}G_{\sigma}^R(\omega)$ , where  $G_{\sigma}^R(\omega)$  is the Fourier transform of the retarded Green's function  $G_{\sigma}^R(t) = -i\Theta(t)\langle\{d_{1\sigma}(t), d_{1\sigma}^\dagger(0)\}\rangle$ . To obtain the most reliable results and quantitatively understand the interplay of strong electron correlations with the presence of Majorana zero-energy modes, we use the numerical renormalization group method [48, 49, 53]. In NRG calculations we use the discretization parameter  $\Lambda = 2$  and keep at least 3000 states at each iteration. Moreover, to increase the accuracy of the spectral functions, which are typically subject to broadening issues [54], we average the data over 4 discretizations [55] and use the optimal broadening method [56]. On the other hand, the results presented for the linear conductance are obtained directly from the discrete NRG data, without the need of resorting to broadening [57].

### III. EFFECTIVE EXCHANGE INTERACTION

In general, the low-temperature transport behavior of a system depends mostly on the low-energy part of the spectrum. In the T-shaped double quantum dot in the presence of normal leads the low-energy states *relevant* for the two-stage Kondo regime are those consisting of two singly-occupied quantum dots, organized into singlet and triplet, split by the effective antiferromagnetic exchange interaction  $J_{\text{eff}} \approx 4t^2/U$  [41]. This structure remains untouched when the device is proximized by the conventional superconductor, only the value of  $J_{\text{eff}}$  increases (irrespective of the geometry) or even  $J_{\text{eff}}$  can arise due to the coupling to a BCS-like superconductor [58]. However, the situation qualitatively changes when the superconductor is topological.

To explore such case, we define the basis states as  $|\chi_1\chi_2n_f\rangle$ , where  $\chi_1$  and  $\chi_2$  are the local states of quantum dots 1 and 2, with  $\chi_i \in \{0, \uparrow, \downarrow, 2\}$ , and the Majorana zero-energy modes are described by the occupation of the auxiliary fermionic operator  $f$ ,  $n_f \in \{0, 1\}$ ; cf. Eqs. (5) and (6). The local Hamiltonian consists then of 32 states, nevertheless, the states relevant for the Kondo regime still consist of half-filled quantum dots. There are

8 such states and we will refer to them as *relevant* states henceforth.

Furthermore, since in the considered model the Majorana mode couples only to one spin channel, the spin  $\mathcal{S}$  is no longer good quantum number, nor are its components. Thus, the structure of the eigenbasis cannot be determined from the spin symmetry requirements. However, the system still exhibits two symmetries, namely, related to the conservation of charge *parity*,  $Q_P = (-1)^Q$  [with  $Q = f^\dagger f + \sum_{j\sigma}(d_{j\sigma}^\dagger d_{j\sigma} - 1/2)$  denoting the negative charge] and the conservation of the number of spin-up electrons,  $N_{\uparrow} = \sum_j d_{j\uparrow}^\dagger d_{j\uparrow}$  [59, 60]. Moreover, for half-filled quantum dots (obtained in the model by setting  $\delta_j = 0$ ) and long Majorana wire ( $\varepsilon_M = 0$ ), the Abelian symmetry related to the  $N_{\uparrow}$  conservation is generalized to the full SU(2) iso-spin symmetry with iso-spin  $z$ -component  $I_z = N_{\uparrow} - 1$ . This symmetry can be easily recognized in the spectrum of the local Hamiltonian. Namely, in this case all the eigenenergies of  $H_{\text{DDM}}$  have the following form

$$E_{\xi\zeta}^I = -\frac{U}{2} \left( 1 + \frac{\xi}{\sqrt{2}} \sqrt{A_I + \zeta\sqrt{B_I}} \right), \quad (8)$$

where indices  $\xi, \zeta$  take values  $\pm 1$  and

$$A_1 = 1 + 4(t^2 + 2V_M^2)U^{-2}, \quad (9)$$

$$B_1 = 1 - 8(t^2 - 2V_M^2)U^{-2} + 16t^2(t^2 + 4V_M^2)U^{-4}, \quad (10)$$

$$A_0 = A_1 + 16t^2U^{-2}, \quad (11)$$

$$B_0 = B_1 + 32t^2U^{-2} + 128t^2(t^2 + 4V_M^2)U^{-4} \quad (12)$$

are constants of the order of unity. The four combinations of signs  $(\xi, \zeta)$ , together with four combinations of iso-spin and its  $z$ -component  $(I, I_z)$  corresponding to  $I \leq 1$ , and double degeneracy due to  $Q_P$ , give all the 32 local states. The lack of dependence of energies on  $I_z$  proves that the symmetry is indeed of SU(2) type. We note that the operators  $I_{\pm}$  can be defined to have non-zero matrix elements only between the degenerated eigenstates of  $H_{\text{DDM}}$  possessing the same charge parity, yet, their explicit form is rather cumbersome.

For  $U \gg t, V_M$ , the order of magnitude of the energies given by Eq. (8) is determined by the signs of  $\xi$  and  $\zeta$ . The lowest energies correspond to  $\xi = +1$  and  $\zeta = +1$ , then  $E_{++}^I \sim -U$ ; the other options lead to  $E_{\xi\zeta}^I \sim -U/2$  or  $E_{\xi\zeta}^I \sim 0$ —up to the terms of the order of  $U^{-2}$ . For the analysis of the low-temperature properties only the former of these are important. Those states, together with their quantum numbers, are listed in Table I. Note, that even though in general the eigenstates do not possess a definite spin  $\mathcal{S}$ , when projected onto the subspace spanned by the *relevant* states (when the coefficients  $m_a$ , defined in Table I, are negligible) they actually do, *i.e.*  $I$  multiplets correspond to  $\mathcal{S}$  multiplets with  $I = \mathcal{S}$ . In general, however, each of the  $(I, I_z)$  eigenstates is a superposition of a single relevant state with  $(\mathcal{S}, \mathcal{S}_z) = (I, I_z)$  and a number of other states, as presented in Table I.

The relation between  $\mathcal{S}$  and  $I$  allows us actually to define the effective exchange interaction as the difference

State	$Q_P$	$I$	$I_z$	Energy
$\alpha_1 s,1\rangle + m_1( 0\uparrow 0\rangle,  \downarrow 20\rangle,  \uparrow 00\rangle,  2\downarrow 0\rangle,  021\rangle,  201\rangle)$	-1	0	0	$E_{++}^0$
$\alpha_2 s,0\rangle + m_2( 0\uparrow 1\rangle,  \downarrow 21\rangle,  \uparrow 01\rangle,  2\downarrow 1\rangle,  020\rangle,  200\rangle)$	+1	0	0	$E_{++}^0$
$\alpha_3 \downarrow\downarrow 1\rangle + m_3( \downarrow 00\rangle,  0\downarrow 0\rangle,  001\rangle)$	-1	1	-1	$E_{++}^1$
$\alpha_4 t,1\rangle + m_4( 0\uparrow 0\rangle,  \downarrow 20\rangle,  \uparrow 00\rangle,  2\downarrow 0\rangle,  021\rangle,  201\rangle)$	-1	1	0	$E_{++}^1$
$\alpha_5 \uparrow\uparrow 1\rangle + m_5( \uparrow 20\rangle,  2\uparrow 0\rangle,  221\rangle)$	-1	1	+1	$E_{++}^1$
$\alpha_6 \downarrow\downarrow 0\rangle + m_6( \downarrow 01\rangle,  0\downarrow 1\rangle,  000\rangle)$	+1	1	-1	$E_{++}^1$
$\alpha_7 t,0\rangle + m_7( 0\uparrow 1\rangle,  \downarrow 21\rangle,  \uparrow 01\rangle,  2\downarrow 1\rangle,  020\rangle,  200\rangle)$	+1	1	0	$E_{++}^1$
$\alpha_8 \uparrow\uparrow 0\rangle + m_8( \uparrow 21\rangle,  2\uparrow 1\rangle,  220\rangle)$	+1	1	+1	$E_{++}^1$

TABLE I. The eight lowest-energy eigenstates of the local Hamiltonian, Eq. (4), obtained for  $\delta_i = \varepsilon_M = 0$  and  $U_1 = U_2 = U$ . For brevity the following notation for the singlet and triplet states,  $|s, n_f\rangle = (|\downarrow\uparrow n_f\rangle - |\uparrow\downarrow n_f\rangle)/\sqrt{2}$  and  $|t, n_f\rangle = (|\downarrow\uparrow n_f\rangle + |\uparrow\downarrow n_f\rangle)/\sqrt{2}$ , was used. The first column presents the corresponding eigenstate, with  $|\alpha_a| \sim 1$  being the coefficient of the *relevant* state and  $m_a$  denoting a superposition of states with coefficients small for  $t, V_M \ll U$ .  $I$  and  $I_z$  stand for the iso-spin quantum numbers. Note, that after neglecting superpositions  $m_a$  the iso-spin  $I$  becomes equivalent to the physical spin  $S$ .

between the energies of the iso-spin singlet and triplet states,

$$\begin{aligned}
J_{\text{eff}} &\equiv E_{++}^1 - E_{++}^0 \\
&= \frac{U}{2\sqrt{2}} \left( \sqrt{A_0 + \sqrt{B_0}} - \sqrt{A_1 + \sqrt{B_1}} \right) \\
&\approx \frac{4t^2}{U} \left[ 1 - \left( \frac{2t}{U} \right)^2 + 2 \left( \frac{2t}{U} \right)^4 - 5 \left( \frac{2t}{U} \right)^2 \left( \frac{2V_M}{U} \right)^2 \right] \\
&\quad + \mathcal{O}(U^{-7}). \tag{13}
\end{aligned}$$

Note that the effect of coupling to topological superconductor becomes relevant only in the fifth order of expansion with respect to  $1/U$ . Clearly, from Eq. (13) one can conclude that the coupling to the Majorana wire slightly decreases the effective exchange interaction between the quantum dots. Interestingly, this effect is opposite to what happens in the presence of a conventional superconductor [58, 61]. Nevertheless, as shown in the following by accurate NRG calculations, the decrease of *bare* exchange interaction becomes overwhelmed by strong electron correlations. Actually, we demonstrate that increasing the coupling to topological wire results in an *enhancement* of the second-stage Kondo temperature  $T^*$  instead of reduction, as one could expect from simple analysis of  $H_{\text{DDM}}$  spectrum, cf. Eq. (13). We note that a similar effect has been predicted for single quantum dots coupled to normal leads and a topological superconductor, where increasing the coupling to Majorana wire gives rise to an enhancement of the Kondo temperature [26, 31, 33, 50]. In the setup considered in this paper, at energy scales below the first-stage Kondo temperature  $T_K$ , the double dot system can be viewed as an effective single quantum dot attached to a conduction band of width  $T_K$  (resulting from Fermi liquid formed by first quantum dot screened by lead conduction electrons) and additionally coupled to Majorana wire. Then, one could expect that increasing the coupling to topological wire would result in an increase of the relevant Kondo temperature (the second-stage Kondo temperature  $T^*$ ), similarly as it does in the case of single quantum dots [26, 31, 33, 50]. This conjecture is corroborated by NRG calculations presented in the following section.

## IV. NUMERICAL RESULTS AND DISCUSSION

We now turn to the numerical analysis of the transport behavior of the considered system. First, we consider the case of long Majorana wire and then also discuss the situation when there is a finite overlap between the Majorana quasiparticles. To uncover the interplay between the Majorana and Kondo physics, we study the behavior of the relevant spin-resolved spectral functions as well as the temperature and gate voltage dependence of the linear conductance through the system.

### A. Spectral functions

The spin-resolved spectral function of the quantum dot directly coupled to the normal leads calculated for different values of the coupling to Majorana wire  $V_M$  and hopping between the quantum dots  $t$  is shown in Fig. 2. In the case of  $V_M = 0$  one observes the conventional two-stage Kondo effect [41, 43], see the first row of Fig. 2. The spectral function first increases with lowering the energy  $\omega$ , which happens for  $\omega \lesssim T_K$ , but then starts to decrease once  $\omega \lesssim T^*$ , where  $T_K$  ( $T^*$ ) is the first-stage (second-stage) Kondo temperature. Because  $T^*$  depends exponentially on the effective exchange interaction  $J_{\text{eff}}$  between the two quantum dots generated by the hopping  $t$  [41, 42, 47],

$$T^* = \alpha T_K e^{-\beta T_K / J_{\text{eff}}}, \tag{14}$$

where  $\alpha$  and  $\beta$  are constants of the order of unity, changing  $t$  results in large changes in  $T^*$ . This is why the region of enhanced conductance for  $T^* \lesssim T \lesssim T_K$  shrinks as  $t$  grows and, e.g. for  $t/U = \Gamma/U = 0.1$ ,  $G(T)$  displays only a small resonance, see Figs. 2(a) and (e). This is characteristic of the *local singlet* regime, where the Kondo effect on the first quantum dot does not develop, but the two dots form a molecular singlet state. The two-stage Kondo regime can be reached from this phase by reducing the hopping  $t$ . We note that even though this is a continuous crossover, it is related to switching on or off many-body

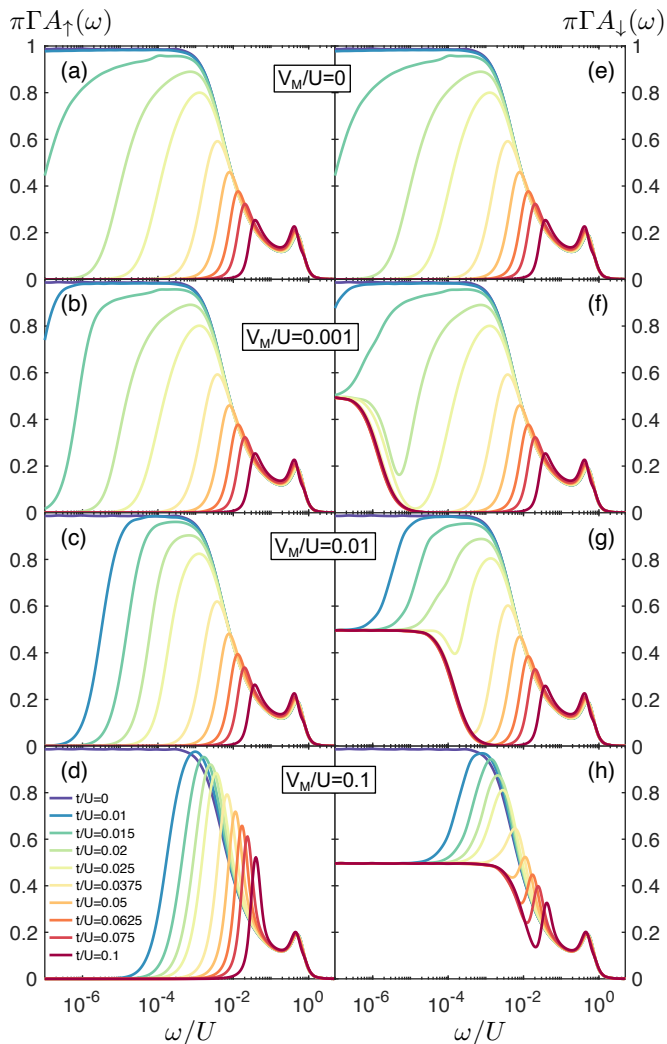


FIG. 2. The normalized spectral function  $\pi\Gamma A_\sigma(\omega)$  of the first quantum dot for (left column) spin-up and (right column) spin-down components calculated for different values of hopping  $t$  between the two dots and the coupling to the Majorana wire  $V_M$ , as indicated. The other parameters are:  $U = 0.2D$ ,  $\varepsilon_1 = \varepsilon_2 = -U/2$  and  $\Gamma = 0.1U$ , where  $D$  is band halfwidth taken as energy unit  $D \equiv 1$ . Note the logarithmic scale on  $\omega$  axis.

Kondo correlations. Namely, for large  $t$  the Kondo effect is absent, while for small values of the hopping between the dots the many-body Kondo state develops. Here we focus on the latter case—as opposed to the Ref. [28].

The behavior of the spectral function changes when the coupling to Majorana wire is present. Note that in the effective Hamiltonian we assumed that only the spin-down component of the dot's spin couples to the Majorana quasiparticles. Thus, the largest effects related to the presence of topological superconductor can be expected in the behavior of  $A_\downarrow(\omega)$ . Nevertheless, finite  $V_M$ , through the Coulomb correlations, also affects the other spin component of the spectral function. For relatively small values of the coupling, see Figs. 2(b) and (f) for

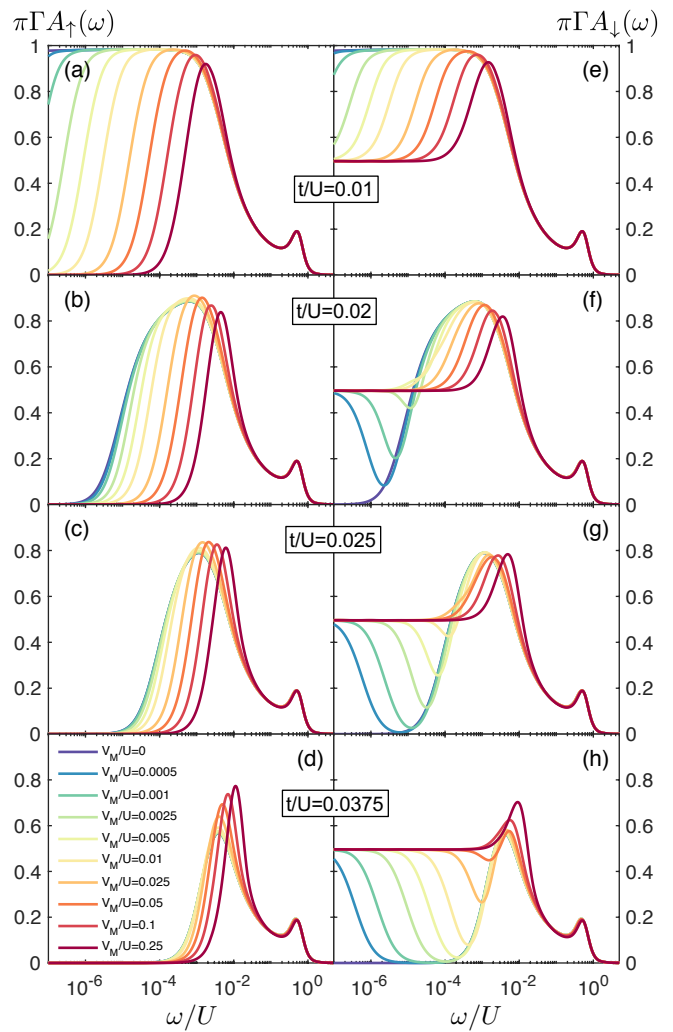


FIG. 3. The same as in Fig. 2 calculated for several values of the hopping between the dots  $t$  while changing the coupling to the Majorana wire  $V_M$ .

$V_M/U = 0.001$ , the low-energy behavior of the spectral function starts changing. For the spin-up component, it is clearly evident that the coupling to Majorana wire strongly affects the second stage Kondo temperature  $T^*$ , i.e.  $T^*$  grows with increasing  $V_M$ . It is also interesting to note that, although  $T^*$  strongly depends on  $V_M$ , the behavior of  $A_\uparrow(\omega \rightarrow 0)$  does not depend on the coupling to the Majorana wire and one has  $A_\uparrow(\omega \rightarrow 0) \rightarrow 0$ .

This is just opposite to the case of the spin-down spectral function, where finite values of  $V_M$  result in  $A_\downarrow(0) = 1/(2\pi\Gamma)$ . Such a fractional value of the spectral function at the Fermi energy is a direct signature of a half-fermionic nature of Majorana quasiparticles. The coupling to Majorana wire *half-suppresses* the second-stage of the Kondo effect at a new energy scale  $\Gamma_M$  resulting from the coupling to topological superconducting wire. As a consequence of this suppression, a five-peak structure can be visible in the spectral function of the first quantum dot for finite  $t$  and  $V_M$ , see e.g. the curve

for  $V_M/U = 0.01$  and  $t/U = 0.05$  in Fig. 2(g).  $A_\downarrow(\omega)$  exhibits the usual Hubbard resonances for  $\omega \approx \pm U/2$  (note that  $\varepsilon_1 = \varepsilon_2 = -U/2$ ). Then, with lowering  $\omega$ ,  $A_\downarrow(\omega)$  starts growing due to the Kondo effect, however, it becomes suppressed once  $\omega \approx T^*$  due to the second-stage Kondo screening, which results in a local maximum around  $\omega \approx T_K$ . With further decrease of  $\omega$  the Majorana energy scale  $\Gamma_M$  comes into play destroying the second-stage Kondo effect and resulting in a further resonance just at the Fermi energy.

All the features discussed above can be also clearly identified in Fig. 3, which presents the spin-resolved spectral functions now plotted for several values of the hopping between the dots  $t$ , while changing the coupling to the Majorana wire  $V_M$ . The enhancement of the second stage of Kondo screening with raising  $V_M$  (due to the increase of  $T^*$ ) can be clearly visible in the left column of Fig. 3. This enhancement is more pronounced when the hopping between the dots is relatively small. As shown in Fig. 3(a), it is the coupling to Majorana wire that actually generates the second-stage of Kondo screening. This is because  $T^*$  for  $t/U = 10^{-2}$  is smaller than the energy scale presented in the figure. However, when  $t$  grows, larger values of coupling to Majorana wire are needed in order to give rise to an increase of  $T^*$ . Nevertheless, the advantageous impact of the coupling to the topological wire on  $T^*$  is clearly visible.

On the other hand, a multi-peak dependence of  $A_\downarrow(\omega)$  due to the leakage of Majorana quasiparticle into the second quantum dot can be seen in the right column of the figure. When the hopping between the dots is relatively small, see Fig. 3(e) for  $t/U = 0.01$ ,  $T^*$  for  $V_M = 0$  is smaller than the energy range considered in the figure and a pronounced Kondo plateau is visible in the spectral function. Turning on the coupling to the Majorana wire, results in a drop of the spectral function to  $1/(2\pi\Gamma)$  at the characteristic energy scale  $\omega \approx \Gamma_M$ , which grows with increasing  $V_M$ . When the hopping between the dots becomes increased, such that the second-stage Kondo screening can be visible in the behavior of the spin-down spectral function shown in Fig. 3, one can observe an interplay between the Kondo effect and Majorana-induced quantum interference. When  $\Gamma_M \lesssim T^*$ , a dip develops in the spectral function and  $A_\downarrow(\omega)$  exhibits a five-peak characteristic dependence, see e.g. Figs. 3(f) and (g). On the other hand, once  $\Gamma_M \gtrsim T^*$ , the dip disappears and  $A_\downarrow(\omega)$  plotted on logarithmic scale shows a plateau of height  $1/(2\pi\Gamma)$  at the Fermi energy.

The second-stage Kondo temperature  $T^*$  and the characteristic Majorana energy scale  $\Gamma_M$  as a function of  $V_M$  are shown in Fig. 4 and plotted for selected values of the hopping between the dots  $t$ .  $T^*$  was estimated as an energy scale at which the spin-up spectral function drops to half of its maximum value with decreasing the energy  $\omega$ . On the other hand, the Majorana energy scale  $\Gamma_M$  was determined from the energy at which the spin-down spectral function drops from  $1/(2\pi\Gamma)$  at  $\omega \rightarrow 0$  to the half of its minimum value as the energy increases. Note

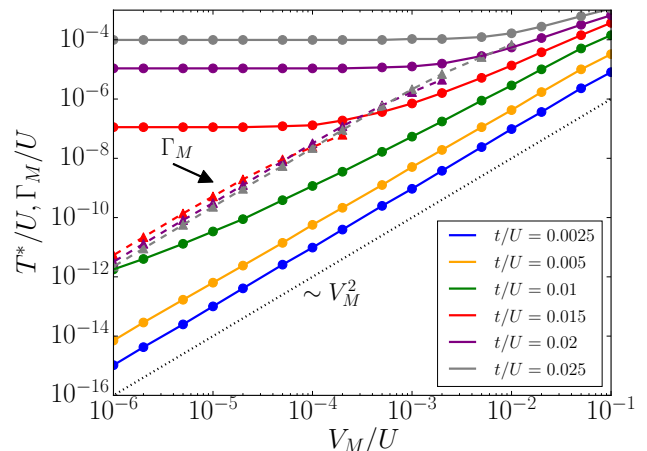


FIG. 4. The second-stage Kondo temperature  $T^*$  and the Majorana energy scale  $\Gamma_M$  plotted as a function of  $V_M$  for several values of the hopping between the quantum dots  $t$ . The other parameters are the same as in Fig. 2. The solid (dashed) line presents  $T^*$  ( $\Gamma_M$ ). Note the logarithmic scale in both axes.

that in this way we can extract  $\Gamma_M$  only for certain range of parameters, i.e. when  $\Gamma_M \lesssim T^*$ .

It can be nicely seen that  $T^* \propto V_M^2$  for low values of hopping between the dots, i.e. when the increase of  $T^*$  is just due to the coupling to Majorana wire, see e.g. the case of  $t/U = 0.0025$  in Fig. 4. However, when  $t$  increases, a larger value of  $V_M$  is needed in order to affect  $T^*$ . Nevertheless, once this happens,  $\Gamma_M$  again scales quadratically with  $V_M$ . On the other hand, if  $T^*$  is relatively large, increasing  $V_M$  does not have any effect on the second-stage Kondo temperature, see the curves for  $t/U \geq 0.015$  for low values of  $V_M$ . In other words, the influence of  $V_M$  on the behavior of  $A_\uparrow(\omega)$  is negligible. This is just contrary to  $A_\downarrow(\omega)$ , which exhibits then new features due to quantum interference with Majorana zero-energy mode, resulting in an additional resonance at the Fermi energy. Actually, the halfwidth of this resonance defines the magnitude of the Majorana energy scale  $\Gamma_M$ . As can be seen in Fig. 4 where  $\Gamma_M$  is presented by dashed lines,  $\Gamma_M \propto V_M^2$ , similarly to  $T^*$ . Note also that the Majorana scale does not depend on the hopping between the dots—the curves presenting  $\Gamma_M$  for different  $t$  overlap, see Fig. 4.

## B. Linear conductance

The interplay between the Majorana and Kondo physics gives rise to well-resolved features visible in the behavior of the linear conductance through the system. First, let us discuss the temperature dependence of  $G$ , whereas later on we will turn to the analysis of the conductance dependence on the gate voltage.

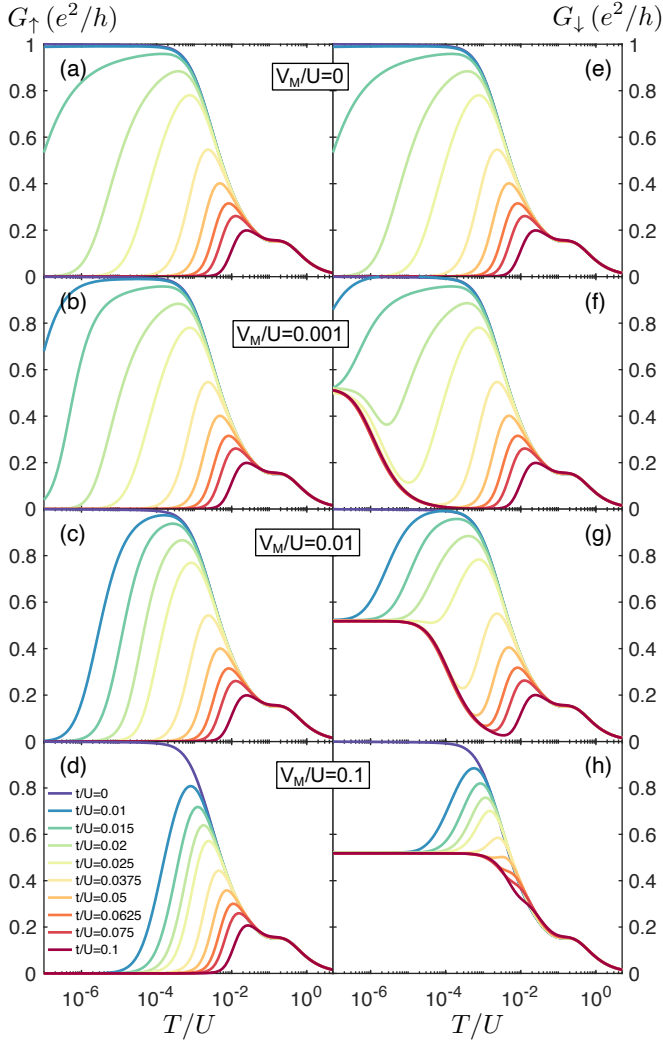


FIG. 5. The temperature dependence of the linear-response spin-resolved conductance through the double dot for (left column) spin-up and (right column) spin-down components calculated for different values of the hopping  $t$  between the dots and the coupling to the Majorana wire  $V_M$ , as indicated. The other parameters are the same as in Fig. 2.

### 1. Temperature dependence

The spin-resolved linear conductance as a function of temperature calculated for different values of hopping between the dots and the coupling to the Majorana wire is presented in Figs. 5 and 6. While the first figure displays  $G(T)$  calculated for selected values of  $V_M$  while tuning  $t$ , the second figure presents a complementary picture:  $G(T)$  determined for a few values of  $t$  while changing  $V_M$ . First of all, we note that the temperature dependence of conductance displays features similar to the energy dependence of the spectral functions. The spin-up component of the linear conductance exhibits a typical nonmonotonic dependence due to the two-stage Kondo effect [41]. First, with lowering the temperature,

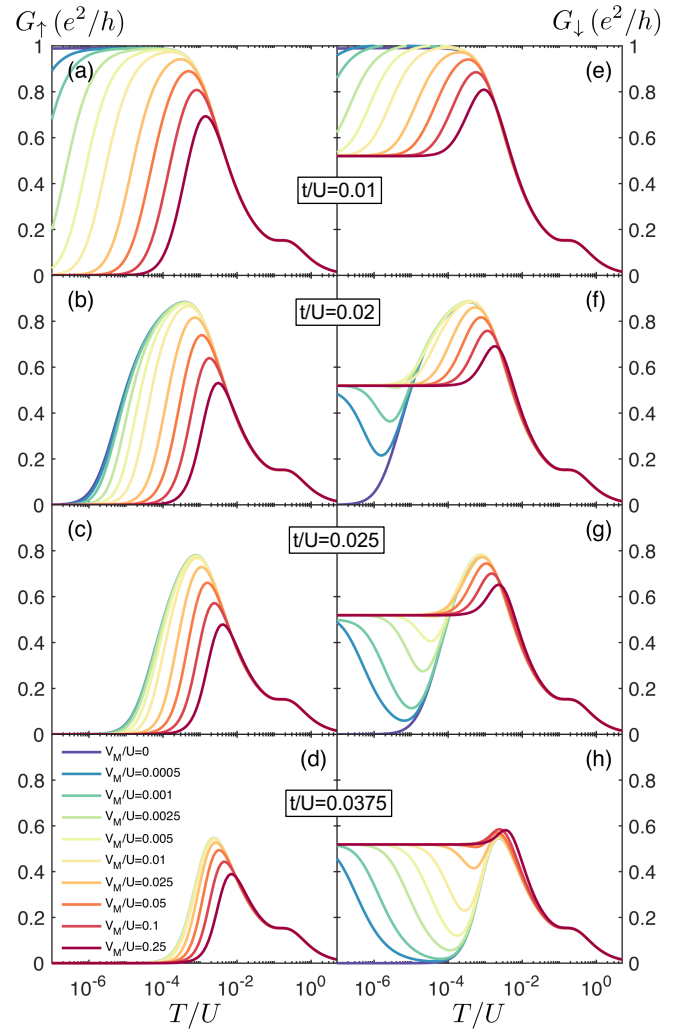


FIG. 6. The same as in Fig. 5, now plotted for selected values of the hopping between the dots  $t$ , while changing the coupling to the Majorana wire  $V_M$ .

the conductance increases due to the Kondo effect, however, around  $T \approx T^*$ , it starts to drop due to the second stage of screening, at which the spin of the second dot becomes screened. Since the second-stage Kondo temperature depends strongly on the coupling to the Majorana wire, increasing  $V_M$  results in an enhancement of  $T^*$ . As a consequence, the maximum value of the conductance, which develops for  $T^* \lesssim T \lesssim T_K$  becomes reduced, see the left columns of Figs. 5 and 6.

On the other hand, the spin-down conductance reveals much richer behavior due to the Majorana-Kondo interplay. It can be seen that when the coupling to the Majorana wire is turned on, the conductance at low temperatures becomes equal to  $G_\downarrow = (1/4)G_0$ . Moreover, the temperature dependence of spin-down conductance strongly depends on the values of  $t$  and  $V_M$ . The quantum interference with the Majorana mode suppresses the second stage of Kondo effect at the energy scale  $T \approx \Gamma_M$ . If the second-stage Kondo temperature  $T^*$  is larger than

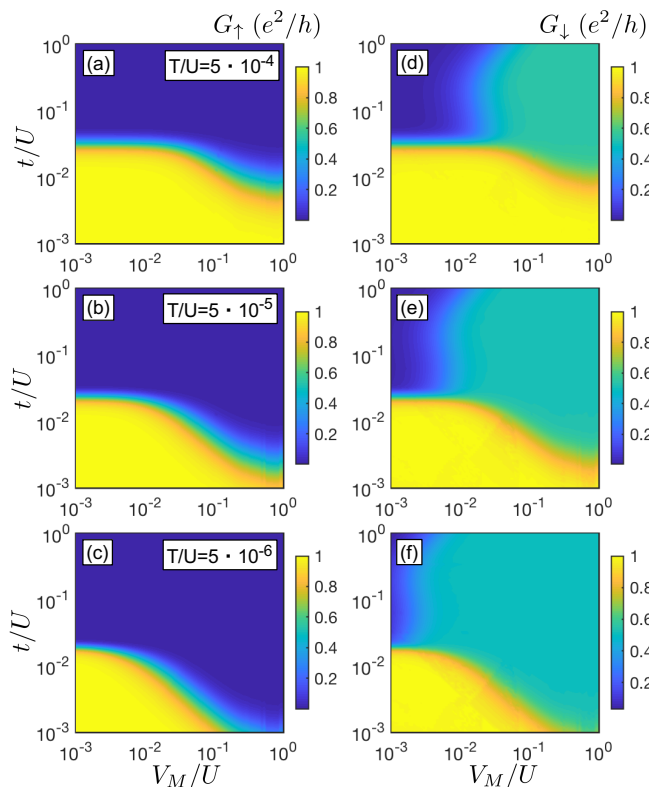


FIG. 7. The linear-response conductance calculated as a function of the hopping between the dots  $t$  and the coupling to the Majorana wire  $V_M$  for different temperatures, as indicated. The left (right) column presents the spin-up (spin-down) contribution. The other parameters are the same as in Fig. 2. Note the logarithmic scale for both  $t$  and  $V_M$ .

$\Gamma_M$ , then the temperature-dependence of  $G_\downarrow$  exhibits a local minimum at  $T \sim T^*$ , see e.g. Figs. 5(f,g) and 6(f)-(h).

While the dependence of conductance on temperature for  $T \gtrsim T_K$  is almost the same for different values of  $t$  and  $V_M$  (for the range of parameters considered in Figs. 5 and 6) the behavior of low-temperature conductance is completely different. Figure 7 presents the linear-response conductance for both spin components calculated at different temperatures while tuning both  $t$  and  $V_M$ . Consider first the spin-up conductance for low-values of  $V_M$ , see the left column of Fig. 7. By increasing the hopping between the dots, the second-stage Kondo temperature becomes enhanced, such that when  $T^* \gtrsim T$ ,  $G_\uparrow$  drops from  $(1/2)G_0$  to 0. Thus, the point when this drop is observed is slightly different in each panel due to a different value of temperature  $T$ . When the coupling to Majorana wire increases, so does the second-stage Kondo temperature  $T^*$ , such that the conductance drop is observed for smaller values of  $t$ . In an extreme situation of very large  $V_M$ , if the temperature is sufficiently low, for all considered values of  $t$  one has  $T < T^*$ , such that the conductance stays suppressed due to the second-stage Kondo effect, see Fig. 7(c) for  $V_M \gtrsim U/10$ . A somewhat similar

behavior can be observed in the spin-down conductance component as far as the regions where  $G_\uparrow = (1/2)G_0$  are concerned, see Fig. 7. This is due to the fact that when the hopping between the two dots is low, such that the second-stage Kondo effect does not develop, the influence of the coupling to the Majorana wire is rather negligible since the Majorana wire is coupled directly only to the second quantum dot. It is therefore clear that the influence of presence of Majorana mode will be most revealed in the parameter regime where the system exhibits the two-stage Kondo effect. Consequently, one observes a completely different behavior in the parameter space where  $G_\uparrow \approx 0$ , cf. the left and right column of Fig. 7. As can be clearly seen, with increasing  $V_M$ , there is a value of  $V_M$  at which the conductance increases from 0 to  $(1/4)G_0$ . At lower temperatures, smaller values of  $V_M$  result in the corresponding change of conductance, which is due to the fact that the condition  $\Gamma_M \gtrsim T$  can be satisfied for smaller values of  $V_M$ .

## 2. Gate voltage dependence

Let us now discuss the gate voltage dependence of the linear-response conductance. In the following we will consider the case when the level of the first quantum dot is tuned, while the level of the second dot is at half filling. The spin-resolved conductance as a function of  $\varepsilon_1$  calculated for selected values of both  $t$  and  $V_M$  at extremely low yet non-zero temperature  $T = 10^{-6}U$  is shown in Figs. 8 and 9. Both spin-up and spin-down conductances exhibit the Kondo plateau for small values of  $t$  and  $V_M$  in the transport regime where the first dot is singly occupied. When the hopping between the dots increases, for  $V_M = 0$ , the Kondo plateau becomes distorted and the conductance suppression develops due to the two-stage Kondo effect, see Fig. 8(a). This suppression becomes more effective when the coupling to Majorana wire is turned on, however, then a clear difference between the spin components shows up. In the spin-up channel, increasing  $t$  and/or  $V_M$ , generally results in larger suppression of the conductance in the singly-occupied first dot regime, i.e. for  $-U \lesssim \varepsilon_1 \lesssim 0$ . This is related to the corresponding increase of  $T^*$ , as already discussed in previous sections. Similarly to the case  $\varepsilon_1 = \varepsilon_2 = -U/2$  considered so far, also for other values of  $\varepsilon_1$  finite coupling to the Majorana wire enhances  $T^*$  and can suppress the conductance through the system; see e.g. Fig. 9(a).

On the other hand, in the case of spin-down conductance one can see that once the second-stage Kondo effect comes into play in the spin-up channel, i.e. suppression of conductance takes place,  $G_\downarrow$  reaches a fractional value of  $(1/4)G_0$ . This is a direct fingerprint of the leakage of Majorana quasiparticle into the attached dot. Consequently, with increasing  $V_M$ , the total conductance saturates at  $(1/4)G_0$ . Moreover, when the coupling to the Majorana wire grows further, this value becomes stabilized in the whole region of the gate voltage and the con-

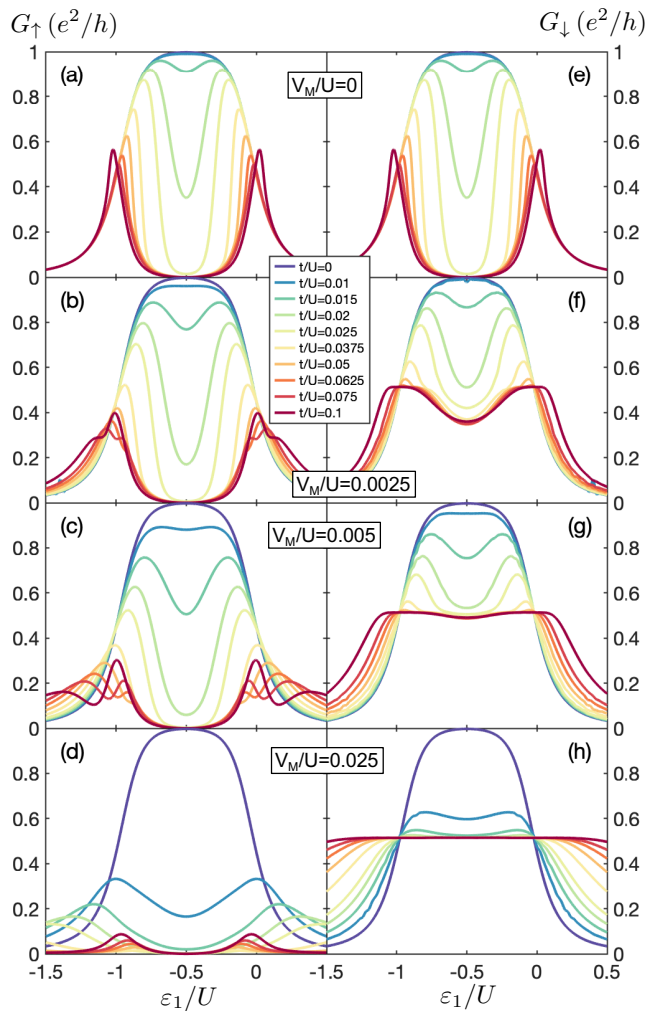


FIG. 8. The conductance plotted as a function of the position of the first quantum dot level  $\varepsilon_1$  for  $\varepsilon_2 = -U/2$  and for selected values the coupling to Majorana mode  $V_M$ , while changing the hopping between the dots  $t$ . The other parameters are the same as in Fig. 2 with  $T = 10^{-6}D$ .

ductance hardly depends on the occupation of the first quantum dot. Similar effect has been predicted for single dots coupled to Majorana wire [26, 31, 33, 50]. Here, we demonstrate that the Majorana zero energy mode can leak through the dot directly coupled to topological superconductor further to the other dot, directly coupled to the normal leads, where it gives rise to fractional values of conductance.

### C. Short Majorana wire case

The interplay between the Majorana and Kondo correlations described in the previous sections can be greatly affected in the case of relatively short topological superconducting wires. Then, a finite overlap between the wave functions of the two Majorana quasiparticles  $\gamma_1$  and  $\gamma_2$ , described by  $\varepsilon_M$ , can emerge. As shown in the follow-

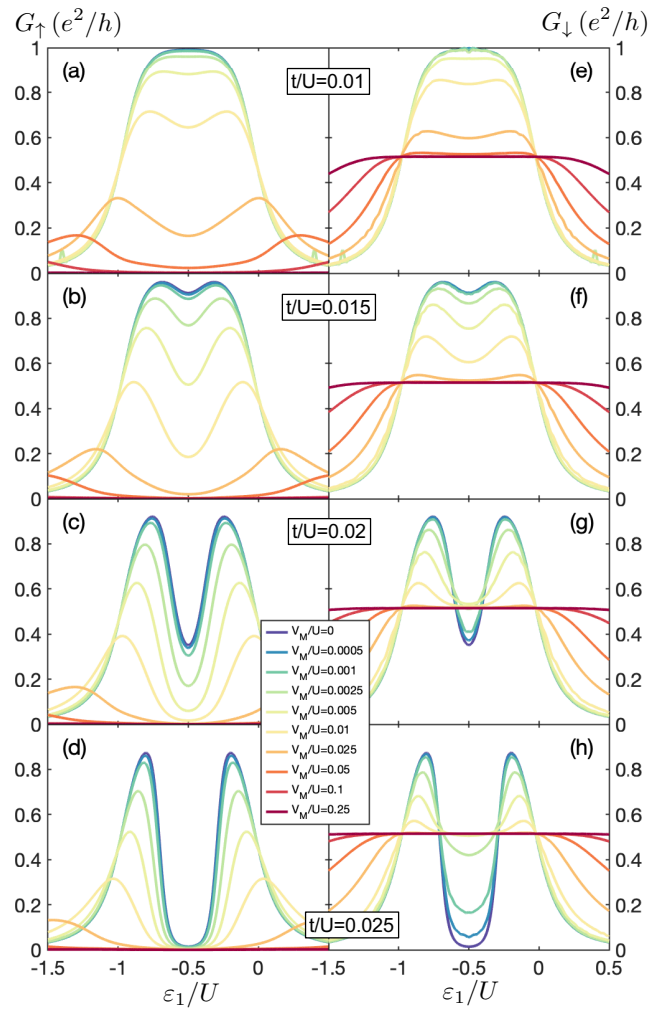


FIG. 9. The same as in Fig. 7, now plotted for selected values of hopping between the dots  $t$ , while changing the coupling to Majorana mode  $V_M$ .

ing, such overlap has a strong influence on the quantum interference responsible for fractional values of the conductance. In fact, such a strong dependence has already been reported theoretically in the case of single quantum dots coupled to external contacts and to the Majorana wire [22, 33, 62, 63]. To examine the influence of the overlap  $\varepsilon_M$  on the transport behavior of the considered double-dot-Majorana setup, in Fig. 10 we show the energy dependence of the spin-resolved spectral function, while Fig. 11 presents the temperature dependence of the linear conductance through the system. These figures were plotted based on calculations performed for selected values of  $\varepsilon_M$  while changing the hopping between the dots and for fixed coupling to Majorana wire,  $V_M/U = 0.01$ . The two figures are complementary in the sense that the temperature dependence of the conductance basically resembles the behavior of the spectral function, except for the fact that some features are smeared out by thermal fluctuations. The case of  $\varepsilon_M = 0$  presented in the first row of Figs. 10 and 11 is just for reference, to help iden-

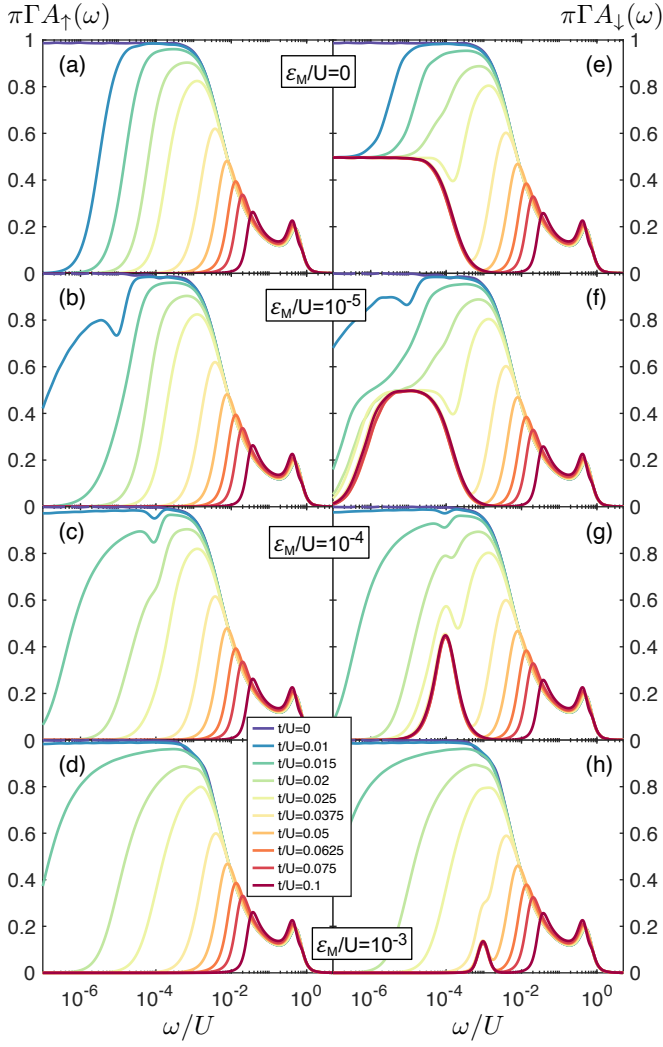


FIG. 10. The normalized spectral function  $\pi\Gamma A_\sigma(\omega)$  for the spin-up (left column) and spin-down (right column) components calculated for different values of the overlap between the Majorana zero-energy modes  $\varepsilon_M$  and the hopping  $t$  between the two dots, as indicated. The parameters are the same as in Fig. 2 with  $V_M/U = 0.01$ .

tifying the impact of finite overlap on the behavior of  $A_\sigma(\omega)$  and  $G_\sigma$ .

The influence of  $\varepsilon_M$  on the spin-up component can be observed in the left column of Figs. 10 and 11. A small local minimum can be seen at the energy scale corresponding to  $\varepsilon_M$ . Interestingly, below this energy scale the interference with the Majorana mode becomes suppressed and the behavior of both  $A_\uparrow(\omega)$  and  $G_\uparrow$  starts resembling that in the case of  $V_M = 0$ . This is especially visible for  $\varepsilon_M/U = 10^{-3}$ , which is presented in Figs. 10(d) and 11(d), where the dependence of the quantities of interest is very similar to that depicted in Figs. 2(a) and 5(a), respectively. Note also that this apparent switching off of the Majorana leakage may lead to additional nonmonotonic behavior of the relevant spectral function if the energy scales happen to fulfill

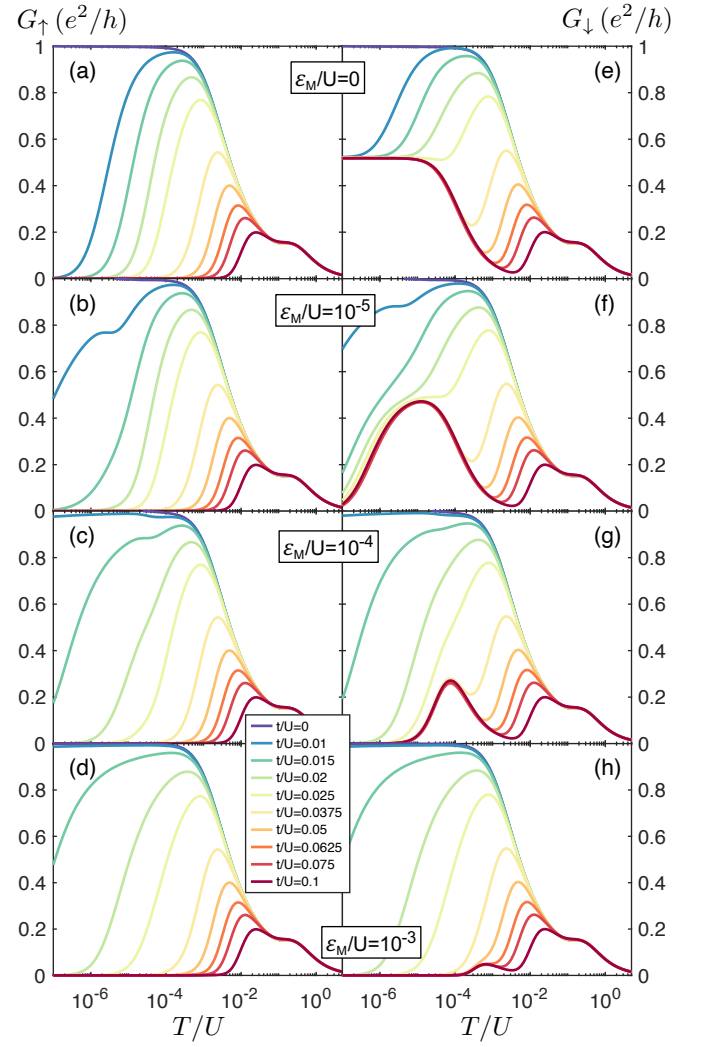


FIG. 11. The linear-response conductance calculated as a function of temperature for different values of the overlap  $\varepsilon_M$  and the hopping between the dots  $t$ , as indicated. The left (right) column presents the spin-up (spin-down) component. The parameters are the same as in Fig. 2 with  $V_M/U = 0.01$ .

$T^*(V_M = 0) < \varepsilon_M < T^*(V_M)$ ; see e.g. the curve for  $t = 0.01U$  in Fig. 11(b).

The destructive influence of the overlap  $\varepsilon_M$  on the quantum interference with Majorana mode is also visible in the spin-down component of both the spectral function and the conductance, which are presented in the right columns of Figs. 10 and 11. Now, a local minimum at the energy scale of  $\varepsilon_M$  can also be observed, see e.g. the case for  $\varepsilon_M/U = 10^{-5}$ . Moreover, below this energy scale the behavior of  $A_\downarrow(\omega)$  and  $G_\downarrow$  becomes comparable to that in the case of  $V_M = 0$ , i.e. the conductance becomes fully suppressed for large  $t$  and  $T \lesssim \varepsilon_M$ . If the overlap is increased further, see the case of  $\varepsilon_M/U = 10^{-3}$ , the behavior of transport quantities resembles that in the absence of coupling to the Majorana wire, except for an additional local maximum visible in both  $A_\downarrow(\omega)$  and  $G_\downarrow$

at the energy scale corresponding to  $\varepsilon_M$ . This result suggests that even strongly overlapping Majorana mode may partially leak into the attached quantum dot.

## V. SUMMARY

In this paper we have examined the transport behavior of a double quantum dot in a T-shaped geometry, side-attached to a topological superconducting wire hosting Majorana zero-energy modes. The considerations were performed by using the numerical renormalization group method, which allowed us to accurately determine the behavior of the spin-resolved spectral functions and the linear-response conductance of the system. We have focused on the transport regime where the system exhibits the two-stage Kondo effect and investigated the influence of the coupling to Majorana wire on this Kondo phenomenon, considering both long and short Majorana wire cases. In the former case, the quantum interference with the Majorana quasiparticle gives rise to a half-suppression of the second-stage of Kondo effect, which results in a fractional value of the low-temperature conductance  $G = (1/4)G_0$ , where  $G_0 = 2e^2/h$ . This phenomenon develops at a new energy scale  $\Gamma_M \propto V_M^2$  associated with the coupling to Majorana wire described by hopping amplitude  $V_M$ . We have shown that the Majorana-Kondo interplay can give rise to an additional resonance in the local density of states for energies lower than the Majorana scale  $\Gamma_M$ . This can be interpreted as a Majorana mode leaking further into the nanostructure, for it determines the low-temperature spectral properties of the first quantum dot, while the Majorana wire is coupled to the second quantum dot. On the other hand, when there is an energy splitting  $\varepsilon_M$  of Majorana modes due to a finite overlap of their wave functions, the quantum interference becomes suppressed and the system exhibits the usual two-stage Kondo effect for energies smaller than  $\varepsilon_M$ . Interestingly, both the conduc-

tance and spectral function exhibit a local maximum at the energy scale corresponding to  $\varepsilon_M$ .

Our findings demonstrate that the low-temperature transport behavior of T-shaped double quantum dots attached to Majorana wires exhibits some unique features due to the leakage of Majorana quasiparticles into the double dot system. First of all, fractional values of the conductance develop in the Majorana-Kondo regime. Moreover, the presence of topological superconductor increases the second-stage Kondo temperature through subtle renormalization effects, even though the relevant local exchange interaction is reduced. On the other hand, in the case of relatively short wires, a local maximum develops in the conductance for temperatures corresponding to the overlap between the two Majorana zero-energy modes. These signatures provide further examples of unique transport behavior due to the presence of Majorana zero-energy modes. Finally, we would like to notice that in the case of considered double quantum dot system the presence of Majorana quasiparticles results in a huge relative change of the low-temperature linear conductance [ $G$  increases from 0 to  $(1/4)G_0$ ], opposite to single dots where the relative change is smaller [ $G$  drops from  $G_0$  to  $(3/4)G_0$ ].

## ACKNOWLEDGMENTS

We thank J. Kroha and E. Vernek for stimulating discussions. This work was supported by the National Science Centre in Poland through the Project No. 2018/29/B/ST3/00937. KPW acknowledges support from the National Science Centre in Poland through project No. 2015/19/N/ST3/01030 and from the Alexander von Humboldt Foundation. PM acknowledges hospitality at University of Bonn. Computing time at the Poznań Supercomputing and Networking Center is warmly appreciated.

- 
- [1] M. Z. Hasan and C. L. Kane, Colloquium: Topological insulators, *Rev. Mod. Phys.* **82**, 3045 (2010).
  - [2] X.-L. Qi and S.-C. Zhang, Topological insulators and superconductors, *Rev. Mod. Phys.* **83**, 1057 (2011).
  - [3] J. Wang and S.-C. Zhang, Topological states of condensed matter, *Nat. Mater.* **16**, 1062 (2017).
  - [4] C. Nayak, S. H. Simon, A. Stern, M. Freedman, and S. Das Sarma, Non-Abelian anyons and topological quantum computation, *Rev. Mod. Phys.* **80**, 1083 (2008).
  - [5] A. Yu. Kitaev, Fault-tolerant quantum computation by anyons, *Ann. Phys.* **303**, 2 (2003).
  - [6] E. Majorana, Teoria simmetrica dell'elettrone e del positrone, *Nuovo Cim.* **14**, 171 (1937).
  - [7] J. Alicea, New directions in the pursuit of Majorana fermions in solid state systems, *Rep. Prog. Phys.* **75**, 076501 (2012).
  - [8] V. Mourik, K. Zuo, S. M. Frolov, S. R. Plissard, E. P. A. M. Bakkers, and L. P. Kouwenhoven, Signatures of Majorana Fermions in Hybrid Superconductor-Semiconductor Nanowire Devices, *Science* **336**, 1003 (2012).
  - [9] M. T. Deng, C. L. Yu, G. Y. Huang, M. Larsson, P. Caroff, and H. Q. Xu, Anomalous Zero-Bias Conductance Peak in a Nb-InSb Nanowire-Nb Hybrid Device, *American Chemical Society* [10.1021/nl303758w](https://doi.org/10.1021/nl303758w) (2012).
  - [10] A. Das, Y. Ronen, Y. Most, Y. Oreg, M. Heiblum, and H. Shtrikman, Zero-bias peaks and splitting in an Al-InAs nanowire topological superconductor as a signature of Majorana fermions, *Nat. Phys.* **8**, 887 (2012).
  - [11] S. M. Albrecht, A. P. Higginbotham, M. Madsen, F. Kuemmeth, T. S. Jespersen, J. Nygård, P. Krogstrup, and C. M. Marcus, Exponential protection of zero modes in Majorana islands, *Nature* **531**, 206 (2016).
  - [12] M. T. Deng, S. Vaitiekėnas, E. B. Hansen, J. Danon,

- M. Leijnse, K. Flensberg, J. Nygård, P. Krogstrup, and C. M. Marcus, Majorana bound state in a coupled quantum-dot hybrid-nanowire system, *Science* **354**, 1557 (2016).
- [13] M.-T. Deng, S. Vaitiekėnas, E. Prada, P. San-Jose, J. Nygård, P. Krogstrup, R. Aguado, and C. M. Marcus, Nonlocality of Majorana modes in hybrid nanowires, *Phys. Rev. B* **98**, 085125 (2018).
- [14] H. Zhang, C.-X. Liu, S. Gazibegovic, D. Xu, J. A. Logan, G. Wang, N. van Loo, J. D. S. Bommer, M. W. A. de Moor, D. Car, R. L. M. Op het Veld, P. J. van Veldhoven, S. Koelling, M. A. Verheijen, M. Pendharkar, D. J. Pennachio, B. Shojaei, J. S. Lee, C. J. Palmstrøm, E. P. A. M. Bakkers, S. D. Sarma, and L. P. Kouwenhoven, Quantized Majorana conductance, *Nature* **556**, 74 (2018).
- [15] R. M. Lutchyn, E. P. A. M. Bakkers, L. P. Kouwenhoven, P. Krogstrup, C. M. Marcus, and Y. Oreg, Majorana zero modes in superconductor–semiconductor heterostructures, *Nat. Rev. Mater.* **3**, 52 (2018).
- [16] Ö. Gül, H. Zhang, J. D. S. Bommer, M. W. A. de Moor, D. Car, S. R. Plissard, E. P. A. M. Bakkers, A. Geresdi, K. Watanabe, T. Taniguchi, and L. P. Kouwenhoven, Ballistic Majorana nanowire devices, *Nat. Nanotechnol.* **13**, 192 (2018).
- [17] D. E. Liu and H. U. Baranger, Detecting a Majorana-fermion zero mode using a quantum dot, *Phys. Rev. B* **84**, 201308 (2011).
- [18] M. Leijnse and K. Flensberg, Scheme to measure Majorana fermion lifetimes using a quantum dot, *Phys. Rev. B* **84**, 140501 (2011).
- [19] Y. Cao, P. Wang, G. Xiong, M. Gong, and X.-Q. Li, Probing the existence and dynamics of Majorana fermion via transport through a quantum dot, *Phys. Rev. B* **86**, 115311 (2012).
- [20] W.-J. Gong, S.-F. Zhang, Z.-C. Li, G. Yi, and Y.-S. Zheng, Detection of a Majorana fermion zero mode by a T-shaped quantum-dot structure, *Phys. Rev. B* **89**, 245413 (2014).
- [21] D. E. Liu, M. Cheng, and R. M. Lutchyn, Probing Majorana physics in quantum-dot shot-noise experiments, *Phys. Rev. B* **91**, 081405 (2015).
- [22] I. Weymann and K. P. Wójcik, Transport properties of a hybrid Majorana wire-quantum dot system with ferromagnetic contacts, *Phys. Rev. B* **95**, 155427 (2017).
- [23] C.-X. Liu, J. D. Sau, T. D. Stanescu, and S. Das Sarma, Andreev bound states versus Majorana bound states in quantum dot-nanowire-superconductor hybrid structures: Trivial versus topological zero-bias conductance peaks, *Phys. Rev. B* **96**, 075161 (2017).
- [24] E. Prada, R. Aguado, and P. San-Jose, Measuring Majorana nonlocality and spin structure with a quantum dot, *Phys. Rev. B* **96**, 085418 (2017).
- [25] A. Ptok, A. Kobińska, and T. Domański, Controlling the bound states in a quantum-dot hybrid nanowire, *Phys. Rev. B* **96**, 195430 (2017).
- [26] G. Górski, J. Barański, I. Weymann, and T. Domański, Interplay between correlations and Majorana mode in proximitized quantum dot, *Sci. Rep.* **8**, 1 (2018).
- [27] J. P. T. Stenger, B. D. Woods, S. M. Frolov, and T. D. Stanescu, Control and detection of Majorana bound states in quantum dot arrays, *Phys. Rev. B* **98**, 085407 (2018).
- [28] J. D. Cifuentes and L. G. G. V. D. Da Silva, Manipulating Majorana zero modes in double quantum dots, *Phys. Rev. B* **100**, 085429 (2019).
- [29] J. F. Silva, L. G. G. V. D. Da Silva, and E. Vernek, Robustness of the Kondo effect in a quantum dot coupled to Majorana zero modes, *arXiv* (2019), 1910.07026.
- [30] E. Vernek, P. H. Penteado, A. C. Seridonio, and J. C. Egues, Subtle leakage of a Majorana mode into a quantum dot, *Phys. Rev. B* **89**, 165314 (2014).
- [31] D. A. Ruiz-Tijerina, E. Vernek, L. G. G. V. Dias da Silva, and J. C. Egues, Interaction effects on a Majorana zero mode leaking into a quantum dot, *Phys. Rev. B* **91**, 115435 (2015).
- [32] A. Golub, I. Kuzmenko, and Y. Avishai, Kondo Correlations and Majorana Bound States in a Metal to Quantum-Dot to Topological-Superconductor Junction, *Phys. Rev. Lett.* **107**, 176802 (2011).
- [33] M. Lee, J. S. Lim, and R. López, Kondo effect in a quantum dot side-coupled to a topological superconductor, *Phys. Rev. B* **87**, 241402 (2013).
- [34] M. Cheng, M. Becker, B. Bauer, and R. M. Lutchyn, Interplay between Kondo and Majorana Interactions in Quantum Dots, *Phys. Rev. X* **4**, 031051 (2014).
- [35] R. Aguado, Majorana quasiparticles in condensed matter, *La Rivista del Nuovo Cimento* **40**, 523 (2017).
- [36] J. Kondo, Resistance minimum in dilute magnetic alloys, *Progress of Theoretical Physics* **32**, 37 (1964).
- [37] A. C. Hewson, *The Kondo problem to heavy fermions* (Cambridge University Press, 1997).
- [38] D. Goldhaber-Gordon, H. Shtrikman, D. Mahalu, D. Abusch-Magder, U. Meirav, and M. A. Kastner, Kondo effect in a single-electron transistor, *Nature* **391**, 156 EP (1998).
- [39] M. Pustilnik and L. I. Glazman, Kondo Effect in Real Quantum Dots, *Phys. Rev. Lett.* **87**, 216601 (2001).
- [40] M. Vojta, R. Bulla, and W. Hofstetter, Quantum phase transitions in models of coupled magnetic impurities, *Phys. Rev. B* **65**, 140405 (2002).
- [41] P. S. Cornaglia and D. R. Grempel, Strongly correlated regimes in a double quantum dot device, *Phys. Rev. B* **71**, 075305 (2005).
- [42] R. Žitko and J. Bonča, Enhanced conductance through side-coupled double quantum dots, *Phys. Rev. B* **73**, 035332 (2006).
- [43] C.-H. Chung, G. Zarand, and P. Wölfle, Two-stage Kondo effect in side-coupled quantum dots: Renormalized perturbative scaling theory and numerical renormalization group analysis, *Phys. Rev. B* **77**, 035120 (2008).
- [44] S. Sasaki, H. Tamura, T. Akazaki, and T. Fujisawa, Fano-Kondo Interplay in a Side-Coupled Double Quantum Dot, *Phys. Rev. Lett.* **103**, 266806 (2009).
- [45] L. G. G. V. Dias da Silva, E. Vernek, K. Ingersent, N. Sandler, and S. E. Ulloa, Spin-polarized conductance in double quantum dots: Interplay of Kondo, Zeeman, and interference effects, *Phys. Rev. B* **87**, 205313 (2013).
- [46] K. P. Wójcik and I. Weymann, Perfect spin polarization in t-shaped double quantum dots due to the spin-dependent fano effect, *Phys. Rev. B* **90**, 115308 (2014).
- [47] K. P. Wójcik and I. Weymann, Two-stage Kondo effect in T-shaped double quantum dots with ferromagnetic leads, *Phys. Rev. B* **91**, 134422 (2015).
- [48] K. G. Wilson, The renormalization group: Critical phenomena and the kondo problem, *Rev. Mod. Phys.* **47**, 773 (1975).

- [49] R. Bulla, T. A. Costi, and T. Pruschke, Numerical renormalization group method for quantum impurity systems, *Rev. Mod. Phys.* **80**, 395 (2008).
- [50] I. Weymann and K. P. Wójcik, Transport properties of a hybrid majorana wire-quantum dot system with ferromagnetic contacts, *Phys. Rev. B* **95**, 155427 (2017).
- [51] K. Flensberg, Tunneling characteristics of a chain of Majorana bound states, *Phys. Rev. B* **82**, 180516 (2010).
- [52] Y. Meir and N. S. Wingreen, Landauer formula for the current through an interacting electron region, *Phys. Rev. Lett.* **68**, 2512 (1992).
- [53] We use the open-access Budapest Flexible DM-NRG code, <http://www.phy.bme.hu/~dmnrg/>; O. Legeza, C. P. Moca, A. I. Tóth, I. Weymann, G. Zaránd, [arXiv:0809.3143](https://arxiv.org/abs/0809.3143) (2008) (unpublished).
- [54] R. Žitko and T. Pruschke, Energy resolution and discretization artifacts in the numerical renormalization group, *Phys. Rev. B* **79**, 085106 (2009).
- [55] V. L. Campo and L. N. Oliveira, Alternative discretization in the numerical renormalization-group method, *Phys. Rev. B* **72**, 104432 (2005).
- [56] A. Freyn and S. Florens, Optimal broadening of finite energy spectra in the numerical renormalization group: Application to dissipative dynamics in two-level systems, *Phys. Rev. B* **79**, 121102 (2009).
- [57] I. Weymann and J. Barnaś, Spin thermoelectric effects in Kondo quantum dots coupled to ferromagnetic leads, *Phys. Rev. B* **88**, 085313 (2013).
- [58] K. P. Wójcik and I. Weymann, Nonlocal pairing as a source of spin exchange and Kondo screening, *Phys. Rev. B* **99**, 045120 (2019).
- [59] R. Bulla and A. C. Hewson, Numerical renormalization group study of the O(3)-symmetric Anderson model, *Z. Phys. B: Condens. Matter* **104**, 333 (1997).
- [60] S. C. Bradley, R. Bulla, A. C. Hewson, and G.-M. Zhang, Spectral densities of response functions for the O(3) symmetric Anderson and two channel Kondo models, *Eur. Phys. J. B* **11**, 535 (1999).
- [61] K. P. Wójcik and I. Weymann, Interplay of the Kondo effect with the induced pairing in electronic and caloric properties of T-shaped double quantum dots, *Phys. Rev. B* **97**, 235449 (2018).
- [62] R. López, M. Lee, L. Serra, and J. S. Lim, Thermoelectrical detection of Majorana states, *Phys. Rev. B* **89**, 205418 (2014).
- [63] I. Weymann, Spin Seebeck effect in quantum dot side-coupled to topological superconductor, *J. Phys.: Condens. Matter* **29**, 095301 (2017).